

Lecture 9 - Dansgaard-Oeschger Events

Henk A. Dijkstra; notes by Gunnar Peng & Chris Spalding

June 25, 2015

1 Dansgaard-Oeschger Events

In previous lectures, we discussed relatively short-term climatic fluctuations in the form of the El Niño Southern Oscillation (ENSO). It is worth asking whether the global climate system possesses similar, apparently stochastic oscillations over longer timescales, so long that no human has lived through an entire cycle and so did not bother to call it an oscillation. In order to seek such climatic modes we must turn to paleoclimatological data. Here, we highlight evidence from ice cores. Specifically, one can drill into the ice on Greenland and extract a core of ice, which has been inexorably laying down layer after layer of annual ice for millennia, recording its local environment as it does so. Bubbles record the paleoatmosphere and this has been used to deduce that, as suspected from its thermal absorption properties, CO₂ has gone down when the ice has gone up, consistent with its greenhouse gas properties. However, it is difficult to use CO₂ as an accurate thermometer. A better thermometer exists in the form of the ratio of “heavy” ¹⁸O to “light” ¹⁶O isotopes within the water molecules of the ice.

The standard way to measure isotope ratios is via the δ -notation defined for oxygen as

$$\delta^{18}\text{O} = \frac{[\text{^{18}O}]/[\text{^{16}O}]_{\text{sample}} - [\text{^{18}O}]/[\text{^{16}O}]_{\text{standard}}}{[\text{^{18}O}]/[\text{^{16}O}]_{\text{standard}}} \times 1000 \quad (1)$$

or, in other words, the measured deviation of the isotope ratio from a given standard multiplied by a thousand, yielding “units” of permil. The lighter isotope of oxygen evaporates more easily and so rain clouds are generally depleted in ¹⁸O relative to seawater. Furthermore, as these rainclouds move towards the poles, where they deposit ice, they rain out even more heavy oxygen ¹ until, by the time they form ice, they are depleted by 10s of permil relative to their source water. The degree of water/vapour fractionation is temperature dependent. Qualitatively, in colder periods, the fractionation is greater, leading to more negative $\delta^{18}\text{O}$ values in ice caps. Additionally, in colder climates, the poles tend to have more ice, which sequesters much of the ocean’s light oxygen, making the ocean heavier in general and the ice caps lighter. Cumulatively, these processes make for *lighter ice caps in colder periods*.

With this theory under our belt, we can look at the measured ice isotope data from Greenland ice cores (Figure 1). Notice first that the record spans about 120,000 years, just long enough to resolve a full “glacial cycle”, i.e., the global oscillation from generally higher

¹This process is known as “Rayleigh Distillation”.

temperatures to generally low temperatures. Records going back much further have revealed that glacial cycles follow such a $\sim 100,000$ year periodicity for at least the previous four cycles. The cause of such a periodicity in glacial cycles is still an active area of research, but here we focus on shorter-scale features, occurring within glacial periods (periods of light ice caps and lower temperatures). Specifically, the ice cores record rapid changes in temperature from cold periods (known as stadiums) to warm periods (interstadials). Between about 70-20 kyr ago, the climate swung abruptly between these states with a periodicity of about 1470 years, with temperature changes up to about 10°C . These transitions have been named Dansgaard-Oeschger (DO) Events and possess a peculiar asymmetry in that the warming phas

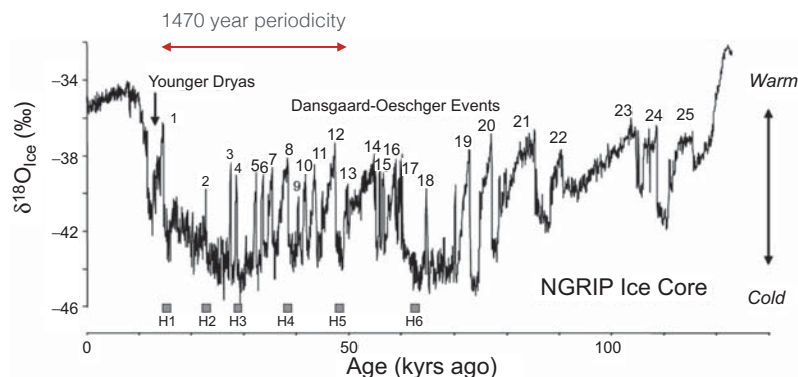


Figure 1: Plot of the $\delta^{18}\text{O}$ data from the NGRIP ice core record. The numbers refer to the interstadials (warm periods, high $\delta^{18}\text{O}$). So-called Heinrich events are marked with the labels H1 to H6. The red arrow denotes the temporal range within which a strong 1470-year periodicity is observed in the $\delta^{18}\text{O}$ signal.

One mysterious feature of DO events is that they don't appear to correspond to any known natural frequency in climatic forcing, as opposed to the glacial cycles themselves which have been linked (with varying degrees of success) to Milankovich Cycles (the Earth's spin-axis precession, obliquity cycles and orbital eccentricity oscillations). The literature exploring the potential sources of DO-events is vast and we do not cover them here. However, what we present is more of a cautionary tale arising out of stochastic theory, namely, that stochastic forcing upon a dynamical system may amplify a periodic signal that you might have otherwise thought negligible, through the process of "Stochastic Resonance". In order to arrive at the key result, we first lay down a theory which allows for multiple stable states within the global overturning and then show how stochastic forcing might cause a system to shift between these states - analogous to DO-events.

1.1 Ocean circulation

Before attempting a dynamical systems description for DO-events, we provide a very brief background on the (Atlantic) Meridional Overturning Circulation, or (A)MOC. Looking at

the Atlantic as whole, there are two main sources of “deep water”, meaning water that more or less descends to the ocean floor by way of negative buoyancy forcing. The first source is Antarctic Bottom Water (AABW), forming, unsurprisingly, near Antarctica. We shall not describe this source in much more detail except to note that it forms the deepest water in the Atlantic by way of extensive cooling in and around the edges of the Antarctic ice sheet. The second source, North Atlantic Deep Water (NADW), is our primary concern here, and more often supposed to be important in driving DO events.

NADW forms mostly in the Greenland and Labrador Seas. Its mechanism of formation is roughly as follows. Strong evaporation at low northern latitudes in the Atlantic increases the surface salinity of the water which is then carried northward into the regions of deep-water formation. The high salinity comes with a high density, which “pre-conditions” the water for convection by eroding its stable stratification. Subsequent cooling in the winter is usually able to destabilise the stratification, leading to deep convection and the formation of deep water. Owing to its high salinity, NADW is actually denser than southern-source AABW *at the surface* of the ocean. However, an interesting property of seawater is that the thermal expansion coefficient increases with pressure, making temperature more important for density at the bottom of the ocean than at the surface. What this amounts to is the coldness of the AABW leading to it being denser than NADW once both have reached the bottom of the ocean. The MOC is often described in terms of a zonally (longitudinally) averaged stream function

$$\Psi_{\text{MOC}}(y, z, t) = \int_z^0 \int_{x_w}^{x_e} v(x, y, z', t) dx dz', \quad (2)$$

where we have chosen $\Psi_{\text{MOC}} = 0$ at the ocean surface and consider a basin with western margin situated at longitudinal position x_w and eastern margin at x_e . The variable y is meridional (latitudinal) distance along the surface of the Earth. Notice that Ψ_{MOC} is a volume transport and is usually measured in Sverdrups (Sv), where $1 \text{ Sv} = 10^6 \text{ m}^3 \text{ yr}^{-1}$. Of interest is the heat carried by this volume, which depends upon the temperature of the northern-ward moving surface water. In general, stronger AMOC correlates with greater heat transport within recent, temporally-limited observations, but it is uncertain to extend this conclusion to longer timescales.

Direct measurements of the MOC are sparse, with a detailed evaluation of Ψ_{MOC} often drawn from numerical models. However, the MOC is now routinely monitored at 23°N using the RAPID-MOCHA array. Essentially, what these observations have revealed is an extremely variable MOC strength, with total transport even appearing to reverse in sign briefly near the beginning of 2010. Paleoproxy evidence has been used to deduce changes to the AMOC in past climate regimes. In particular, the ratio of ^{231}Pa to ^{230}Th in Atlantic sediments has been used to deduce a dramatic and sudden switching off of the AMOC roughly 18 kyr ago, coinciding with Heinrich Stadial 1 (H1, figure 1). The AMOC appears to have abruptly switched back on again about 14,700 kyr ago, at the start of a period of warming known as the Bølling-Allerød interstadial (McManus et al. 2004). We do not have evidence for such transitions during all DO events, but the knowledge that the AMOC can change so dramatically warrants further investigation into whether multiple stable states might be inherent to the system.

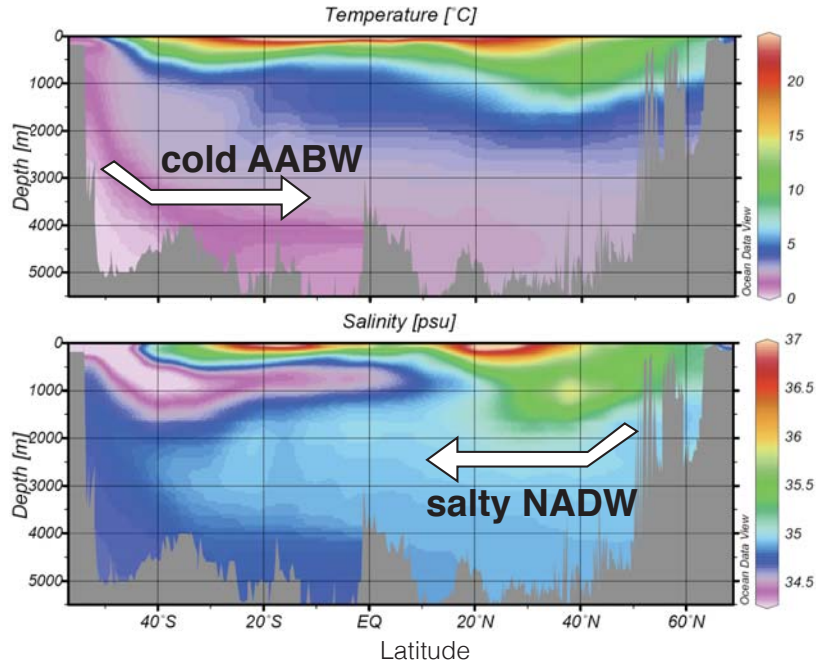


Figure 2: A section along the Atlantic. The top diagram shows the measured salinity and the lower depicts (potential) temperature. Water sinks to deep levels in the North and the South, as can be seen in the sections as a salty tongue descending from the north and a cold tongue from the south. At the ocean floor, the southern-source AABW is denser, by virtue of its low temperature than the northern-sources NADW, which is warmer. Variability in the associated heat transport from the northern regions has been implicated in the origin of DO events.

1.2 The salt - advection feedback

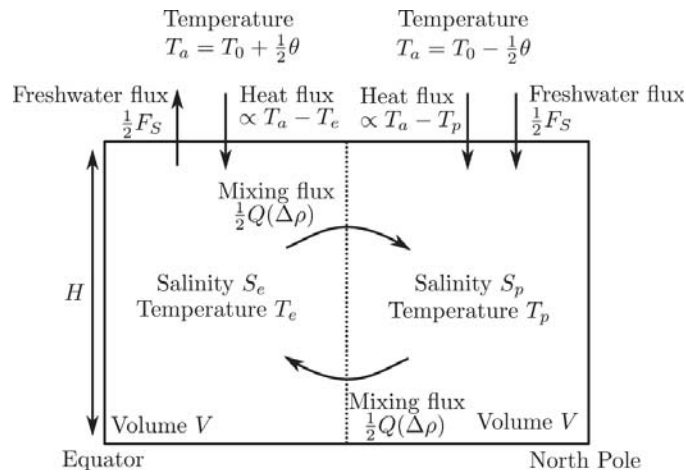


Figure 3: Stommel two-box model of salt-advection feedback.

The simplest picture one can imagine that captures the key aspects of the AMOC can be traced back to Stommel (1961). It is reasonable to suppose that the degree of mixing between equatorial and polar water reservoirs depends upon their mutual density difference $\Delta\rho$. A physical reason for this is that denser polar water is more pre-conditioned to convect to the ocean floor, enhancing meridional overturning and presumably pole-equator mixing. Accordingly, we begin the formulation of our simple model by supposing there to exist two reservoirs of water, one representing the poles and the other the equator, with temperatures and salinities T_p, S_p and T_e, S_e respectively (see figure 3).

We approximate the density of seawater as following a simple linear dependence upon T and S ,

$$\rho = \rho_0 - \alpha_T(T - T_0) + \alpha_s(S - S_0), \quad (3)$$

where the thermal expansivity α_T and salinity coefficients α_s are assumed constant. We may then express the density difference between the two reservoirs as

$$\Delta\rho = -\alpha_T(T_p - T_e) + \alpha_s(S_p - S_e), \quad (4)$$

which in turn governs the mixing rate $Q(\Delta\rho)$.

These two reservoirs not only interact with each other, but are individually forced at their boundaries. Specifically, we suppose the temperature to relax, over a timescale t_r , to the local atmospheric temperature T_a . In the interest of symmetry, we suppose the polar box to possess $T_{a,p} = T_0 - \theta/2$ and the equatorial box to relax to $T_{a,e} = T_0 + \theta/2$. Salinity, too, is forced. However, a crucial aspect of atmosphere-ocean interactions is that, whereas colder water will have greater tendency to draw in heat than warmer water, salty water does not stimulate the atmosphere to rain on it! Consequently, salinity forcing is poorly modelled as a relaxation to some equilibrium value. We adopt a more physical form for the forcing whereby a prescribed flux $F_s/2$ of fresh water enters the polar ocean (in the form of rain, meltwater, etc.), with an equal volume (for simplicity) leaving at the equator by evaporation. As S_0 is the typical value of salinity in the ocean, the result of the freshwater flux is a decrease in salinity in the polar box with rate proportional to $F_s S_0$ and an equivalent increase in the equatorial box.

We may now write out the equations governing the two-basin system (see Cessi 1994):

$$\dot{T}_e = -\frac{1}{t_r}[T_e - (T_0 + \frac{1}{2}\theta)] - \frac{Q(\Delta\rho)}{2}(T_e - T_p), \quad \dot{S}_e = +\frac{F_s}{2H}S_0 - \frac{Q(\Delta\rho)}{2}(S_e - S_p) \quad (5a)$$

$$\dot{T}_p = -\frac{1}{t_r}[T_p - (T_0 - \frac{1}{2}\theta)] - \frac{Q(\Delta\rho)}{2}(T_p - T_e), \quad \dot{S}_p = -\frac{F_s}{2H}S_0 - \frac{Q(\Delta\rho)}{2}(S_p - S_e) \quad (5b)$$

where H is the ocean depth. We can now see that in the form written above, $Q(\Delta\rho)$ must be positive. The reason for this is that although Q is physically the advection of water between two reservoirs, this advection is closed, with as much going in as is coming out for each reservoir. If you reverse the direction of circulation the quantity of polar water moving into the equator and vice versa remain unchanged. With this in mind, considering the simplicity of the model, we are free to choose a functional form for Q that depends only on the magnitude of $\Delta\rho$. For definiteness, we choose

$$Q(\Delta\rho) = \frac{1}{t_d} + \frac{q}{\rho_0^2 V}(\Delta\rho)^2, \quad (6)$$

where V is the volume of each reservoir, q is a dimensional transport coefficient and t_d is the timescale of diffusive mixing between the two reservoirs that would occur in the absence of a density difference.

We are interested in obtaining the possible steady state solutions to the system of equations above and so it is convenient to define the temperature and salinity differences

$$\Delta T \equiv T_e - T_a, \quad \Delta S \equiv S_e - S_a \quad (7)$$

and work in terms of these variables. From equations 5, we obtain the time evolution of the temperature and salinity differences:

$$\frac{d\Delta T}{dt} = -\frac{1}{t_r}(\Delta T - \theta) - Q(\Delta\rho)\Delta T, \quad (8a)$$

$$\frac{d\Delta S}{dt} = \frac{F_s}{H}S_0 - Q(\Delta\rho)\Delta S. \quad (8b)$$

We now introduce appropriate scales with which to reduce the dynamical variables ΔT and ΔS , together with time t , to their respective dimensionless forms. Appropriate choices are as follows

$$x \equiv \frac{\Delta T}{\theta}, \quad y \equiv \frac{\alpha_s \Delta S}{\alpha_T \theta}, \quad t' \equiv \frac{t}{t_d}. \quad (9)$$

Once scaled, the dynamical equations for $x(t')$ and $y(t')$ read

$$\dot{x} = -\alpha(x - 1) - x[1 + \mu^2(x - y)^2], \quad (10a)$$

$$\dot{y} = F - y[1 + \mu^2(x - y)^2], \quad (10b)$$

where

$$\alpha = \frac{t_d}{t_r}, \quad \mu^2 = \frac{qt_d(\alpha_t\theta)^2}{V}, \quad F = \frac{\alpha_s S_0 t_d}{\alpha_t \theta H} F_s. \quad (11)$$

The parameter α is the ratio of the diffusive timescale to the timescale over which temperature would exponentially decay to the local atmospheric value. The parameter μ measures the strength of the buoyancy-driven convection between the two basins relative to the diffusive mixing. The parameter F measures the amount of freshwater forcing.

Parameter	Meaning	Value	Unit
t_r	temperature relaxation timescale	25	days
H	mean ocean depth	4,500	m
t_d	diffusion time scale	180	years
t_a	advection time scale	29	years
q	transport coefficient	1.92×10^{12}	m^3s^{-1}
V	ocean volume	$300 \times 4.5 \times 8,250$	km^3
α_T	thermal expansion coefficient	10^{-4}	K^{-1}
α_S	haline contraction coefficient	7.6×10^{-4}	–
S_0	reference salinity	35	g kg^{-1}
θ	meridional temperature difference	25	K

Table 1: Parameters of the stochastic salt advection model.

We may simplify the equation above by noting that for parameters typical of the real ocean (see table) $\alpha \gg 1$, which means that the reservoirs will equilibrate with their local forcing temperatures much more rapidly than they are likely to mix each other's temperatures. Therefore, we may suppose that x remains close to 1 which reduces the problem to an ODE in $y(t)$ alone (where we drop the primes on t' for convenience):

$$\frac{dy}{dt} = F - y [1 + \mu^2(1 - y)^2]. \quad (12)$$

If we suppose for now that $F = \bar{F}$ is independent of time, we can represent the time evolution of y using a potential function $V(y)$:

$$\frac{dy}{dt} = -V'(y), \quad \text{where } V(y) = -\bar{F}y + \frac{1}{2}y^2 + \mu^2 \left(\frac{1}{4}y^4 - \frac{2}{3}y^3 + \frac{1}{2}y^2 \right), \quad (13)$$

and its derivative with respect to y is denoted by the prime. We illustrate $V(y)$ using $\bar{F} = 1.1$ and $\mu^2 = 6.2$ in Figure 4. As can be seen, $V(y)$ is a double-welled potential with two stable minima and an unstable maximum. In order to transition from one potential well to the other, a finite amplitude “kick” in y is required.

Recalling that y is simply the dimensionless salinity difference, we immediately see that the two reservoirs can remain in a stable state with either a large salinity difference or a small one. Physically, these correspond to the following. The poles are colder and fresher than the equator. If we freshen the poles, we increase ΔS , but because temperature drives the convection, this freshening reduces $\Delta\rho$ and so the MOC weakens. Therefore, the higher (lower) value of y is usually referred to as the off (on) state of circulation. Another way to look at it is that in order to balance the freshwater forcing at a large ΔS we need less mixing between the reservoirs than if we have a smaller ΔS . Ultimately, the conclusion here is that the meridional overturning circulation can jump between the on and off states impulsively, given a finite-amplitude forcing, such as a particularly large ice-melt event.

Of course, freshwater forcing F is unlikely to be constant in reality. Next, we consider F to vary stochastically, perhaps modelling rainstorms, or ice-sheet collapses, which create a set of random kicks of freshwater flux which we model as white noise with amplitude σ such that $F = \bar{F} + \sigma\xi(t)$. This leads to the stochastic Itô equation

$$dY_t = -V'(Y_t) dt + \sigma dW_t. \quad (14)$$

Note here that the result of adding fluctuations to F is additive noise in the equation for Y , rather than noise in the potential $V(y)$.

As we have seen in previous lectures, we can write down the forward Fokker-Planck equation in order to solve for the probability density function $p(y, t)$ that generates a given trajectory in Y_t

$$\frac{\partial p}{\partial t} = \frac{\partial}{\partial y} \left(V'(y)p \right) + \frac{1}{2}\sigma^2 \frac{\partial^2 p}{\partial y^2}. \quad (15)$$

Now, in the deterministic case before, we sought time-independent solutions for y . Of course, it makes no sense to look for truly time-independent solutions for the random variable Y_t , but a *statistically steady* solution may be found by setting $\partial p/\partial t = 0$ and

solving for the function $p^{\text{stat}}(y)$ satisfying stationary statistics. The solution is relatively straightforward and we simply state the result,

$$p^{\text{stat}}(y) = C e^{-\frac{2}{\sigma^2} V(y)}, \text{ where } C = \left(\int_{-\infty}^{\infty} e^{-\frac{2}{\sigma^2} V(y)} dy \right)^{-1} \quad (16)$$

is the normalization coefficient and we have used the boundary condition that $p \rightarrow 0$ as $y \rightarrow \pm\infty$.

Some numerical results for equations 14 and 15 are shown in figure 4. The histograms and probability densities are initially peaked at the well near which the system was launched, indicating that the peak at $y = y_b$ is difficult to cross. They do eventually spread out, though, and attain the steady state given by equation 16. In this state, the system typically fluctuates around in one of the two wells and randomly transitions between them, while spending more time overall in the deeper well.

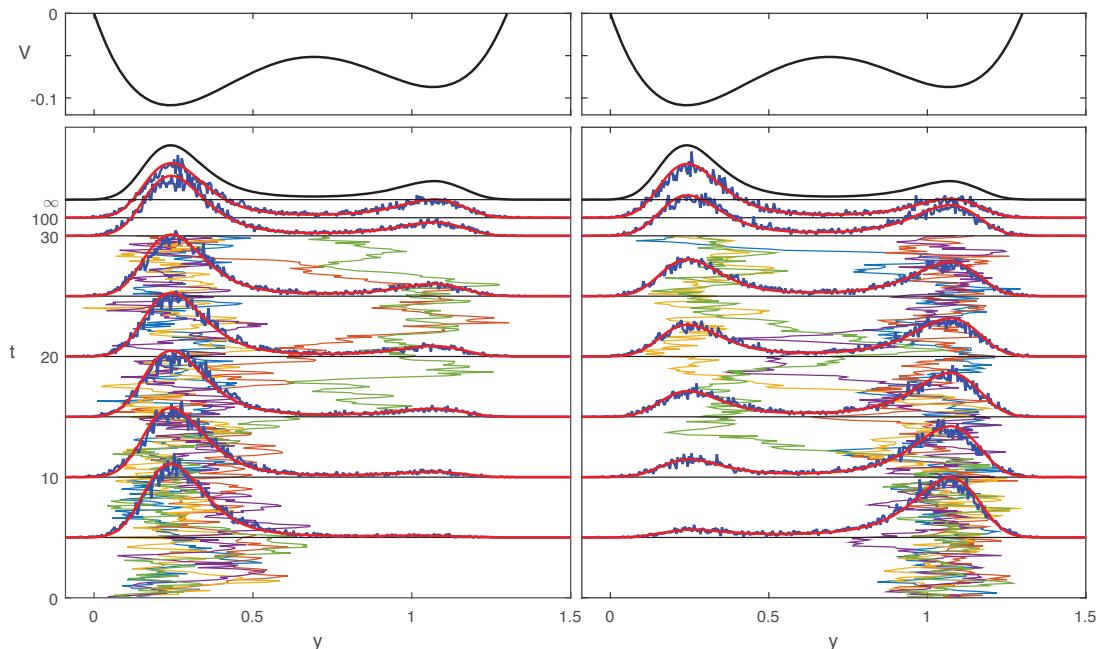


Figure 4: Motion in the double-well potential $V(y)$ from equation 13 with $\bar{F} = 1.1$ and $\mu^2 = 6.2$. Top: Potential $V(y)$. Bottom: Stochastic motion (equation 14) with noise amplitude $\sigma = 0.2$ starting from $Y_0 = 0$ (left) or $Y_0 = 1$ (right). The time evolution of five realizations are shown, as well as histograms (blue) from 10 000 realizations and the probability density (red) obtained from numerical solution of the corresponding Fokker–Planck equation (15). The distribution labelled $t = \infty$ is the steady-state distribution $p^{\text{stat}}(y)$ from equation 16.

1.3 Escape time

We discussed in a previous lecture the concept of mean escape times. In this context, suppose we are in the “on”-state $y = y_a$ of meridional overturning but subject the system to given, stochastic freshwater forcing. How long is it likely to take for the system to flip into the other (“off”) state $y = y_c$?

The expected time $\bar{T}(y)$ required to escape to y_c when starting from y satisfies an equation related to the backward Kolmogorov equation:

$$-1 = -V'\bar{T}' + \frac{1}{2}\sigma^2\bar{T}'', \quad \text{with} \quad \bar{T}(y_c) = 0, \quad \bar{T}'(-\infty) = 0, \quad (17)$$

where the boundary conditions state that it takes no time to reach y_c when starting from y_c , and that the escape time varies very little for y far below the potential well at y_a since the restoring deterministic drift is very strong there.

The equation is a linear first-order equation for $\bar{T}'(y)$ which we solve by multiplying by the integrating factor $\exp(-2V(y)/\sigma^2)$:

$$-e^{-\frac{2}{\sigma^2}V} = e^{-\frac{2}{\sigma^2}V} \left(-V'\bar{T}' + \frac{\sigma^2}{2}\bar{T}'' \right) = \frac{\sigma^2}{2} \left(e^{-\frac{2}{\sigma^2}V}\bar{T}' \right)'. \quad (18)$$

Integration of both sides and using the boundary condition $\bar{T}'(-\infty) = 0$ yields

$$\bar{T}'(y) = e^{\frac{2}{\sigma^2}V(y)} \int_{-\infty}^y -\frac{2}{\sigma^2} e^{-\frac{2}{\sigma^2}V(s)} ds = -\frac{2}{\sigma^2} \int_{-\infty}^y e^{\frac{2}{\sigma^2}[V(y)-V(s)]} ds. \quad (19a)$$

A second integration using $\bar{T}(y_c) = 0$ yields

$$\bar{T}(y) = -\frac{2}{\sigma^2} \int_{z=y_c}^y \int_{s=-\infty}^z e^{\frac{2}{\sigma^2}[V(z)-V(s)]} ds dz. \quad (20)$$

Hence the mean escape time from the “on” state $y = y_a$ to the “off” state $y = y_c$ is

$$\boxed{\bar{T}(y_a) = \frac{2}{\sigma^2} \int_{z=y_a}^{y_c} \int_{s=-\infty}^z \exp\left(\frac{2}{\sigma^2}[V(z) - V(s)]\right) ds dz.} \quad (21)$$

1.3.1 Asymptotic approximation using Laplace’s method

We can obtain an asymptotic approximation to the above integral in the limit of small noise, where σ^2 is much smaller than the typical variation $V(y_b) - V(y_a)$ of the potential, so that we can treat $M = 2/\sigma^2$ as a large parameter. In this case, the main contribution to the integral in equation 21 comes from the region where the exponent $M[V(z) - V(s)]$ is maximal, i.e. $z \approx y_b$ and $s \approx y_a$. The contributions from any other regions are exponentially small and can be ignored. We can thus approximate the result as

$$\bar{T}(y_a) \approx M \int_{y_b-\epsilon}^{y_b+\epsilon} e^{MV(z)} dz \int_{y_a-\epsilon}^{y_a+\epsilon} e^{-MV(s)} ds, \quad (22)$$

where $\epsilon > 0$ is small.

After a change of variables $z = y_b + x$ or $s = y_a + x$, the two integral factors in equation (22) have the form

$$I \equiv \int_{-\epsilon}^{\epsilon} e^{Mf(x)} dx, \quad (23)$$

where $M \gg 1$ and $f(x) = V(y_b + x)$ or $f(x) = -V(y_a + x)$ has a maximum at $x = 0$. We have argued that almost all of the contribution to the integral I comes from the region near this maximum, so we may Taylor expand $f(x)$ as $f(x) \approx f(0) + f''(0)x^2/2$, where no linear term is present and $f''(0) < 0$ since $x = 0$ is a maximum. After the expansion, we can extend the limits to infinity, again because the contributions from regions away from the exponential maximum near $x = 0$ are negligible, and hence

$$\int_{-\epsilon}^{\epsilon} e^{Mf(x)} dx \approx e^{Mf(0)} \int_{-\epsilon}^{\epsilon} e^{-\frac{1}{2}M|f''(0)|x^2} dx \quad (24a)$$

$$\approx e^{Mf(0)} \int_{-\infty}^{\infty} e^{-\frac{1}{2}M|f''(0)|x^2} dx \quad (24b)$$

$$\approx e^{Mf(0)} \sqrt{\frac{2\pi}{M|f''(0)|}}, \quad (24c)$$

where we have made use of the standard result $\int_{-\infty}^{\infty} e^{-\alpha x^2} dx = \sqrt{\pi/\alpha}$.

The two integral factors in equation 22 are thus

$$\int_{y_b-\epsilon}^{y_b+\epsilon} e^{MV(z)} dz \approx \sqrt{\frac{2\pi}{M|V''(y_b)|}} e^{MV(y_b)}, \quad (25a)$$

$$\int_{y_a-\epsilon}^{y_a+\epsilon} e^{-MV(s)} ds \approx \sqrt{\frac{2\pi}{M|V''(y_a)|}} e^{-MV(y_a)}, \quad (25b)$$

and hence the mean escape time from the “on” state $y = y_a$ to the “off” state $y = y_c$ is approximately

$$\bar{T}(y_a) = 2\pi \sqrt{\frac{1}{|V''(y_a)||V''(y_b)|}} \exp\left(\frac{2}{\sigma^2} [V(y_b) - V(y_a)]\right). \quad (26)$$

From the calculations, we can see that this escape time is the same from any state in the well near $y = y_a$ over the peak $y = y_b$ to any state in the well near $y = y_c$. This is in line with our intuition that, for weak noise, the deterministic drift quickly drives the system to the bottom of the well $y = y_a$ where it fluctuates until eventually a large enough random perturbation kicks the system over the crest $y = y_b$ and it falls into the other well $y = y_c$.

1.4 Periodic forcing

Within the autonomous framework above, the system will jump between on and off states stochastically, but will not display any periodic behaviour, as is observed for DO events.

We therefore augment the previous model with a periodic modulation to the deterministic part of the freshwater forcing, so that

$$F = \bar{F} + \sigma\xi(t) + A \sin\left(2\pi\frac{t}{T}\right), \quad (27)$$

where A is the amplitude of periodic forcing and T is the dimensionless period of forcing (as we are still working with dimensionless variables). The governing equation is thus $dy/dt = -dV/dy + \sigma\xi(t)$, where the potential $V(y, t)$ can be chosen as

$$V(y, t) = -\bar{F}y + \frac{1}{2}y^2 + \mu^2\left(\frac{1}{4}y^4 - \frac{2}{3}y^3 + \frac{1}{2}y^2\right) - A \sin\left(2\pi\frac{t}{T}\right)(y - 0.7). \quad (28)$$

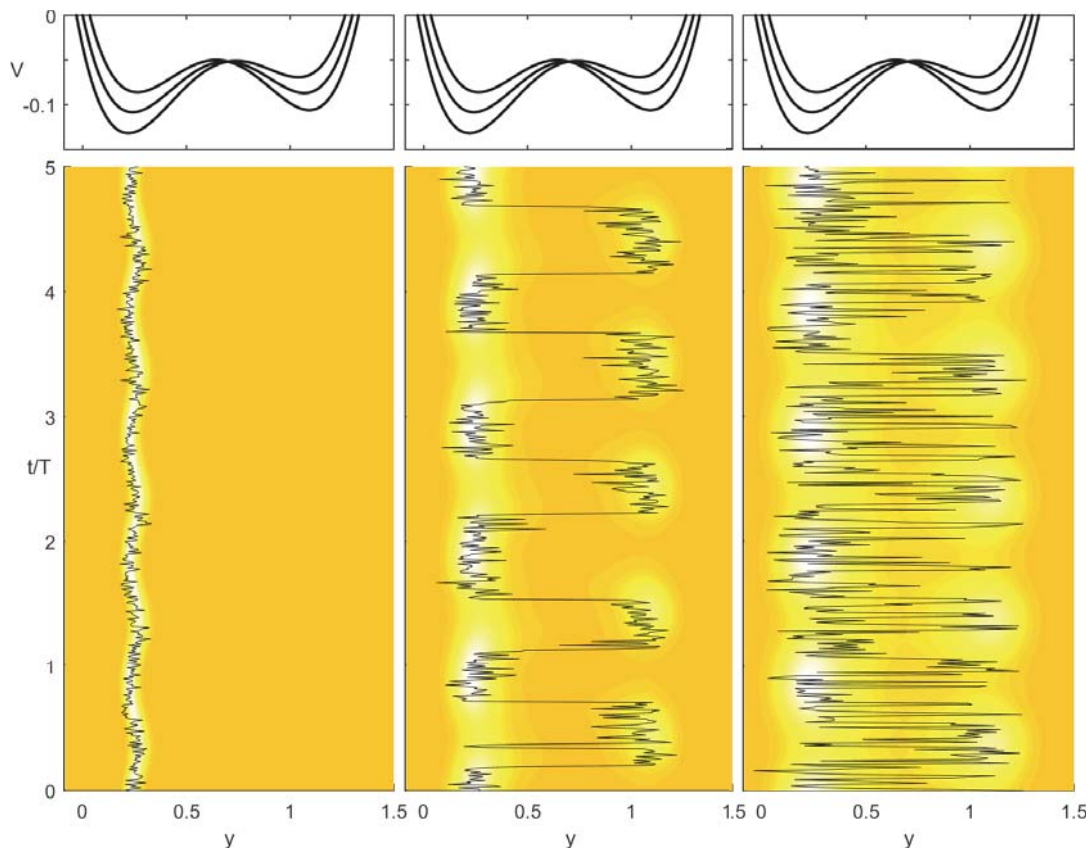


Figure 5: Motion in a time-periodic double-well potential (equation 28 with $\bar{F} = 1.1$, $\mu^2 = 6.2$ and $A = 0.05$). Top: The potential V at $t = -T/2, 0, T/2$. Bottom: Stochastic motion with noise amplitude $\sigma = 0.05$ (left), $\sigma = 0.15$ (middle), $\sigma = 0.25$ (right). The time evolution of one realization is shown (black curve), as well as the probability density (heat map) obtained from evolving the corresponding Fokker–Planck equation forward until a time-periodic state is reached. The period T chosen corresponds to 100 000 years.

In Figure 5, we show what happens for a small perturbation ($A = 0.05$) to the mean forcing \bar{F} for various values of the noise amplitude σ . For small noise, the system remains

in the deeper well most of the time as expected. For large noise, the probability density system frequently transitions between the two wells, almost as if the middle peak at $y = y_b$ did not exist, and the periodicity is quite weak. However, for an intermediate value of noise strength, we recover periodic behaviour on the timescale T . The response is not a small perturbation, but a jump between on and off states every cycle. We have ended up with a system exhibiting so-called “**stochastic resonance**”, whereby the noise is just large enough to switch between states almost every time the background forcing oscillates.

It is unclear whether the DO events are in fact generated by such a mechanism (the addition of a ~ 1500 year periodicity in freshwater forcing is *ad hoc* – we know of no such forcing in reality), but it nonetheless constitutes a fascinating result that ordered behaviour may come out of the addition of white noise.